Kinetics of ferroelectric domains investigated by scanning force microscopy

V. Likodimos, M. Labardi, and M. Allegrini*

INFM, Unità di Pisa-Università, Via F. Buonarroti 2, I-56127 Pisa, Italy

(Received 22 October 1999)

Voltage-modulated scanning force microscopy has been applied to investigate domain kinetics in triglycine sulfate single crystals, thermally quenched from the paraelectric to the ferroelectric phase. Temporal analysis of the equal-time correlation functions shows that the average domain size grows initially with a power law dependence close to that of conserved systems, whereas a crossover to the slower logarithmic growth law $L(t) \propto [\ln(t/t_0)]^4$ predicted for systems with random impurities occurs in the late stage of coarsening. Domain growth is dominated by a single characteristic length scale consistent with the dynamical scaling hypothesis. The total surface charge corresponding to the domain area of the two polarization states is found to be conserved within the studied time scale, indicating that the system may be considered to behave like one with conserved order parameter.

I. INTRODUCTION

Investigations of the domain structure and its dynamical evolution are essential from both fundamental and applied perspective since they determine to a large extent the macroscopic response of ferroelectric materials.[1,2] To reveal ferroelectric domain structures, several experimental methods have been developed such as optical techniques, surface etching, colloidal decoration, pyroelectric techniques, x-ray topography, nematic liquid crystal method, and electron microscopy.[3] These methods, however, may suffer from stringent experimental and sample preparation conditions and usually exhibit limited spatial resolution. Significant progress in the investigation of domain structures has been recently accomplished exploiting advances in scanning probe techniques[4–6] as well as in environmental scanning electron microscopy.[7] In particular, scanning force microscopy (SFM) has emerged as a powerful, nondestructive method to visualize ferroelectric domains as well as to control them with nanoscale resolution.[8] The domain structure in uniaxial ferroelectric single crystals such as triglycine sulfate (TGS) has been distinguished with high lateral resolution in various SFM operation modes, the underlying contrast mechanism relying on the diverse surface potentials and the different surface morphology produced by selective etching of oppositely polarized ferroelectric domains,[9–12] the pronounced electrostatic force gradient at domain boundaries,[5,13–16] and the response to an external modulation voltage due to electrostatic and piezoelectric effects.[4,17–21]

When a ferroelectric single crystal is quenched from the disordered paraelectric phase into the ordered ferroelectric one, a fine domain pattern is formed satisfying the requirement for minimal energy of the depolarizing fields which originate from discontinuities of the spontaneous polarization occurring at the crystal surfaces or in the vicinity of defects.[3] With the passage of time, the domain structure gradually becomes coarse. The temporal evolution of the domain patterns is considered as an asymptotic process to an equilibrium domain configuration reflecting the decrement in the electrostatic energy by charge compensation for the spontaneous polarization. In this respect, domain coarsening

in ferroelectric materials can be treated within the framework of phase-ordering kinetics addressing the growth of order in a system subjected to a quench from the homogeneous to a broken-symmetry phase.[22,23] The best known example of such behavior is the spinodal decomposition of binary mixtures where the order parameter, the concentration, is conserved and domains grow with a power law dependence.[22] More recently, liquid crystals, where the length and time scale of domain growth is readily accessible by conventional optical microscopy, have offered fertile experimental ground for testing theoretical predictions in various systems.[24] A central feature of domain kinetics is the scaling hypothesis implying that at late times of domain growth there is a dominant single length scale $L(t)$ in the ordering process such that the domain patterns become independent of time when the corresponding lengths are scaled by $L(t)$.[23] The time dependence of the characteristic length scale, known as the growth law, depends critically on the nature of the order parameter and spatial dimensionality of the system, as well as the presence of conservation laws.[22,23] In the case of ferroelectric systems undergoing a symmetry-breaking transition from the disordered to an ordered phase, induced either by a rapid thermal quench (phase transition) or the application of an electric field (polarization reversal), the dynamical evolution of the domain structure can be considered to originate from the rise of nuclei of different dimensionality.[25] The appearance of new domains corresponds to three-dimensional nuclei, while the growth of domains can be attributed to the arising of one- and two-dimensional nuclei at the already existing domain walls.[25]

Recently, the domain structure of triglycine sulfate, which is a very well known ferroelectric,[3] has been intensively investigated employing various SFM operation modes.[9–15,17–21] TGS undergoes a second-order phase transition at the *Curie* temperature of $T_c \approx 49\,°\mathrm{C}$ with the vector of spontaneous polarization along the polar b axis. On cooling from the paraelectric to the ferroelectric phase, 180°-oriented domain walls form separating regions of opposite polarity, whose preferential orientation, nearly perpendicular to the c axis, is attributed to the anisotropic wall energy.[26] The temporal evolution of the TGS domain structure has been mainly

investigated by the etching method[27,28] and the nematic liquid crystal (NLC) method[29–31] both employing for domain detection conventional optical microscopy whose spatial resolution is, however, confined by diffraction. Earlier etching and NLC measurements performed either at room temperature or just below the Curie point have consistently shown that the mean domain width increases linearly with time.[27–29] More recent NLC studies, where the spatial correlation functions of the TGS domain patterns with respect to time were derived, revealed that the characteristic domain length increases according to a definite power law.[30,31] The total surface charge was found to be conserved in the studied time scale and the dynamical scaling law was shown to be valid.[30,31] Most of the recent SFM studies have been mainly concerned with investigations of the static TGS domain structure and the exploration of the underlying contrast mechanism. In spite of this significant progress, domain kinetics on the nanometer scale afforded by SFM has been explored to a much lesser extent,[13–15,20,21] while no quantitative information on domain coarsening has been reported so far.

In this work, we have exploited scanning force microscopy employing modulation techniques to investigate domain coarsening dynamics in real time and on the submicron scale for TGS single crystals quenched from the paraelectric to the ferroelectric phase. In order to probe the temporal evolution of the domain structure, the equal-time correlation functions have been analyzed, yielding the time dependence of the characteristic correlation length. The average domain size is thus found to increase in the early stage of coarsening with a power growth exponent close to that for conserved systems, whereas a crossover to the logarithmic power growth law characteristic of random pinning forces occurs in the late stage of coarsening. Domain growth is found to proceed based on a single length scale consistently with dynamical scaling, while surface charge is found to be conserved within the investigated time scale.

II. EXPERIMENTAL METHOD

SFM measurements were performed using the voltage-modulation technique.[17–21] The method is based on the application of an ac voltage between the conductive tip and a metallic sample holder, resulting in mechanical vibrations of the cantilever due to electrical-electromechanical effects.[32] The presence of a finite vibration amplitude in the contact region has been recently detected and accordingly the corresponding measurement mode has been termed as dynamic contact electrostatic force microscopy (DC-EFM),[20,21] an abbreviation adopted hereafter in order to discriminate it from the conventional noncontact EFM mode, though it disregards the presence of electromechanical effects. The main advantage of this operation mode is that strong domain contrast can be obtained with no essential correlation with topographic features, which may interfere in domain images acquired in the noncontact or friction operation modes. In particular, the cantilever deflection employed as the feedback signal is still determined by the dominant repulsive atomic forces as in the usual contact mode, thus ensuring the deconvolution of topographic properties from the electric ones which are detected by the highly sensitive lock-in technique.
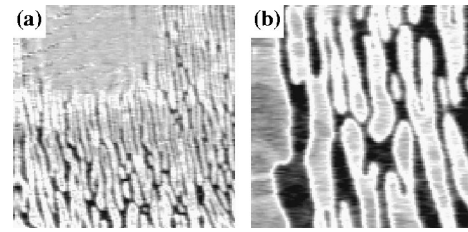

FIG. 1. DC-EFM images of ferroelectric domains on the TGS (010) surface thermally quenched from 60 °C to 43 °C. The images correspond to the amplitude signal and they are recorded (a) 3 min and (b) 368 min, after crossing T_c. Scan size 14×14 μm², ac voltage frequency $f = 78.8$ kHz.

Although the DC-EFM mode allows an unambiguous identification of ferroelectric domains, controversy still remains as to the origin of the underlying domain contrast mechanism. In the linear response signal, which is the usual detection configuration, domain contrast is assumed to arise either from the electrostatic interaction[20,21] and/or the converse piezoelectric response of the ferroelectric sample under the action of the ac voltage.[18,19,32] In a recent work, we have identified a frequency-induced variation of domain contrast and the presence of resonance effects in DC-EFM.[33] The latter effect, which can be associated with the mechanical resonance of the coupled tip-sample system excited by the ac electric field, has been exploited in the present measurements for the optimization of detection conditions.

Measurements were performed in ambient atmosphere using a home-built SFM,[34] recently implemented to a DC-EFM.[35] Conductive ($\rho \sim 0.01\Omega$ cm) n^+-doped silicon cantilevers (Nanosensors) with resonance frequencies of about 15 kHz and nominal spring constants of about 0.1 N/m were used. Topography detection is based on the optical lever method and stable operation is established in the constant force mode. The frequency (f) of the ac voltage is in the range of 10–100 kHz with peak-to-peak amplitude of 15 V. The cantilever deflection signal is fed to a dual lock-in amplifier so that the amplitude and phase as well as the in-phase and out-of-phase components of the perpendicular oscillations can be recorded simultaneously with the topographic image. Temperature-dependent measurements were carried out employing a home-built temperature controller integrated in the microscope head.[35] Thin slices (thickness ≈ 0.6 mm) of a TGS single crystal grown from aqueous solution were cleaved in air parallel to the ac plane. The specimen was fixed with conducting copper paste on a metallic sample holder, while contact electrification was avoided by the presence of an insulating oxide layer on the surface of the probe tip. Thermal treatment of the sample has been performed *in situ* on the microscope heating-cooling stage.

III. RESULTS AND DISCUSSION

A. Domain coarsening in quenched TGS

Figures 1(a) and 1(b) show the domain images corresponding to the amplitude signal for the (010) surface of a TGS specimen which was subjected to thermal annealing at 60 °C for 60 min and then rapidly cooled at a rate of 4 °C/min, to 43 °C. The domain image, recorded a few minutes after the sample has crossed T_c, reveals a fine lamellar
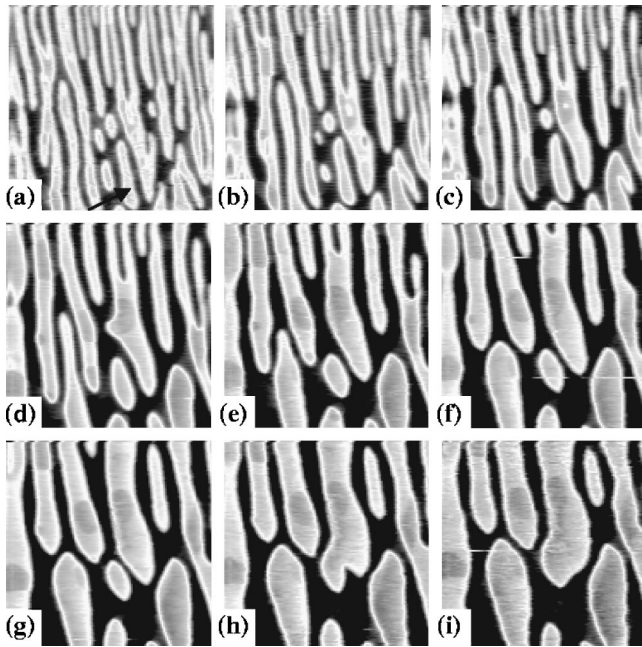
FIG. 2. Domain images, recorded sequentially up to 360 min at 43 °C, of the TGS (010) surface after quenching from 60 °C. The images correspond to the amplitude signal and are recorded at time intervals of (a) 5 min, (b) 15 min, (c) 30 min, (d) 60 min, (e) 125 min, (f) 185 min, (g) 237 min, (h) 300 min, and (i) 360 min. Scan size 7×7 μm^2, $f = 78.8$ kHz.

domain pattern comprising mainly elongated domains of irregular shape along with smaller nuclei both embedded in the surrounding matrix of opposite polarity, as shown in Fig. 1(a). Such a domain configuration complies with the lamellar domain patterns, running through the crystal thickness, reported for TGS after annealing above the Curie point, rather than spikelike, nonthrough domains with lenticular cross section in the ac plane.[36] The domain image of the same area 365 min later, shown in Fig. 1(b), exhibits a much coarser domain structure indicative of a substantial temporal evolution, though the pattern looks statistically similar to the initial one, implying the possibility of the presence of dynamical scaling. In both cases, sharp domain contrast is observed, allowing an unambiguous identification of the ferroelectric domain structure, the only correlation with topography being the faint contrast of the upper left part of the initial image [Fig. 1(a)], which is caused by a circular surface protrusion. Such topographic distortions in domain images may arise from the local variation of the tip-sample distance by prominent topographic features, which may affect both the tip-sample capacitance[20] and the local piezoelectric response.

The temporal evolution of the domain ordering process within the same time interval, was traced by taking a sequence of domain images corresponding to the amplitude signal at frequency f, in higher magnification (7×7 μm^2) of the central part of Fig. 1(a), with constant recording conditions. Figure 2 shows examples of TGS domain images taken sequentially up to 360 min at 43 °C, where the origin of time is referred to the time of the first observation of the domains, corresponding to Fig. 1(a). The frequency of the applied ac voltage was 78.8 kHz which is close to the resonance peak of the response amplitude signal yielding, apart from the strong contrast between the two domain states, an
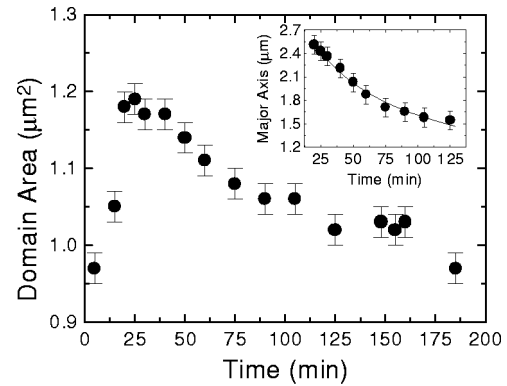

FIG. 3. Temporal evolution of the domain area of the elongated domain depicted by arrow in Fig. 2(a). The inset shows the time dependence for the major axis of the domain, while the solid line corresponds to the fit to a power law of the form $R(t) \propto (t - t_0)^{\phi}$ with $t_0 = -22(9)$ min and $\phi = 0.43(11)$.

enhanced domain wall contrast which is imposed as brighter lines at the domain boundaries visible in Fig. 2. Determination of the image contrast by histogram analysis of the corresponding images as a function of time reveals a substantial increase, from 0.50 up to 0.80, within the first 30 min and then remains approximately constant. Given the present experimental conditions, namely, the tip-sample-rear electrode configuration along with the formation of intervening surface dielectric layers in the ambient environment, screening of the depolarization fields by bulk and surface charge,[37] corresponding to an intermediate regime of internal and external screening respectively,[25,38] is likely to occur in the investigated time scale. Taking into account that domain contrast in DC-EFM is determined by the competition of electrostatic and piezoelectric effects[32] and the presence of surface screening charge, it might be possible that the observed contrast enhancement reflects a compensation process for the spontaneous polarization at the initial time interval.

Domain pattern ordering mainly proceeds by the shrinking of the elongated domains and smoothing of the curved domain interfaces, thus implying a dominant curvature-driven growth mechanism stemming from surface tension that is realized in the case of ferroelectric domains by an equivalent electric field exerted on domain walls.[39] Minute domains observed at the early stages of coarsening rapidly shrink until they vanish [Figs. 2(a)–2(c)], while coalescence of adjacent domains also occurs followed by contraction of the protruding boundaries [Figs. 2(d)–2(f)]. Figure 3 shows the temporal evolution of the area for the small, initially elongated, domain depicted by the arrow in Fig. 2(a). The domain contracts continuously along the major axis and evolves towards a lenticular shape, while the curved boundaries become smoother with the passage of time (Fig. 2). During approximately the first 30 min, the domain area increases and subsequently decreases roughly linearly with time (Fig. 3) until coalescence with the adjacent elongated domain occurs, as shown in Figs. 2(h)–2(i). A similar temporal variation of the domain diameter has been reported in a recent DC-EFM study of TGS, for small domains embedded in larger elongated domains, which, however, did not show any temporal evolution.[20] The initial growth may be caused by the shrinkage of the smaller domains in the vicinity of the
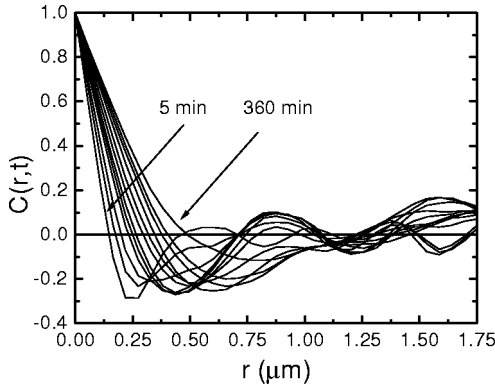
FIG. 4. Equal-time correlation function $C(r,t)$ as function of r computed along the horizontal direction of the TGS domain patterns, at different times $t=5$, 15,25, 40, 50, 75, 105, 148, 185, 237, 300, 360 min.

specific domain, which vanish in the same time interval. In this case, the current produced by the polarization reversal of the smaller domains, which in the presence of screening will correspond to a screening current, flows into the neighboring domain boundaries, causing enhancement of the domain area. Fitting of the temporal variation of the major axis with a power law of the form $R(t) \propto (t-t_0)^{\phi}$ in the time interval of 25–125 min yields $t_0 = -22(9)$ min and $\phi = -0.43(11)$. The fitting curve is shown in the inset of Fig. 3. Although the time dependence of $R(t)$ for the single domain does not comply with a t^{-1} behavior anticipated from a linear temporal variation, the limited number of data points does not allow a precise determination of the relative exponent.

B. Growth law

In order to probe the ordering dynamics of the observed domain patterns, we employ the equal-time correlation function defined as $C(r,t) \equiv \langle S(r,t)S(0,t) \rangle$, where $S(r,t)$, corresponding to the scalar order parameter field, assumes the values of $+1$ and -1 for r inside a ''white'' or ''black'' domain, respectively, reflecting the two opposite polarization states, while the brackets denote the spatial average.[23] Optimization of image contrast was performed by applying background removal. Subsequently, images were converted into binary matrices (128×128) after using a threshold filter, and $C(r,t)$ was calculated along the horizontal image direction, perpendicular to the domain walls, which corresponds closely to the crystallographic c axis. Figure 4 shows the resulting correlation functions as a function of r, for different times. For short distances, $C(r,t)$ decreases rapidly with r, while as the distance increases oscillations appear in the tail of $C(r,t)$, indicative of periodicity along the horizontal direction (c axis) in the observed lamellar pattern. In the initial ordering stage, the correlation functions decay rapidly within a short distance interval, reflecting the very fine domain structure. The decay of $C(r,t)$ with distance becomes much slower with the passage of time, as a result of substantial coarsening of the domain structure. It is worth noting that both the shape and temporal evolution of the derived $C(r,t)$ agree with previous NLC studies of TGS domain patterns consisting mainly of isolated lenticular domains.[30,31]

In order to trace the growth law for the observed patterns we examine the temporal evolution of the characteristic
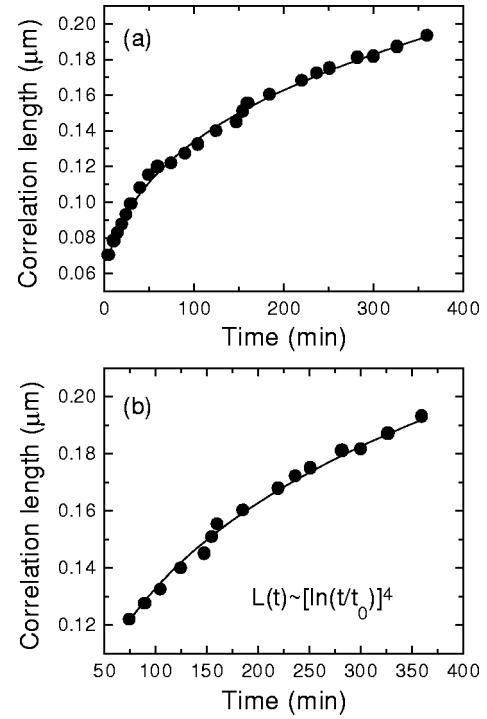

FIG. 5. (a) Time dependence of the characteristic correlation length $L(t)$ within a time interval of 360 min. The solid line corresponds to the best fit curve to the power law $L(t) \propto (t-t_0)^{\phi}$ with $t_0 = -7(1)$ min and $\phi = 0.295(9)$. (b) The fit of $L(t)$ in the late stage of coarsening, to the logarithmic growth law $L(t) \propto [\ln(t/t_0)]^4$.

length scale $L(t)$ defined as the distance where $C(r,t)$ becomes half of its value at $r=0$, i.e., $C[r=L(t),t]=1/2$, for a given time t. Figure 5(a) shows the time dependence of the characteristic correlation length $L(t)$ calculated from the domain patterns at 43 °C within a time interval of 360 min. The correlation length $L(t)$ exhibits a rapid increase at the early stage of domain evolution, which becomes slower in the later stage. This behavior has been fitted to a power law $L(t) \propto (t-t_0)^{\phi}$ with best fit values $t_0 = -7(1)$ min and $\phi = 0.296(9)$. The correponding fitting curve is shown in Fig. 5(a). The negative value of t_0 indicates that nucleation of domains has occurred before the time of the first observation which was assumed as our reference time. The exponent value determined from the fit of $L(t)$ is in good agreement with the corresponding ϕ values (0.32 and 0.29) reported from the NLC studies of TGS domain coarsening on the submilimiter range.[30,31] The derived exponent value of 0.3 deviates considerably from the purely curvature-driven growth law with $\phi = 1/2$ expected for nonconserved systems, while it is much closer to the usual $\phi = 1/3$ growth exponent for conserved systems with scalar order parameter.[23,40] However, a closer inspection of the data shows that a more precise fit may be obtained for $L(t)$ in two different time regimes. Specifically, in the early stage ($t \leq 60$ min), $L(t)$ can be fit to the power growth law with $\phi = 0.39(4)$, which is still closer to that of conserved than nonconserved dynamics, whereas a crossover to a much slower growth rate with $\phi = 0.28(2)$ occurs at the later growth stage ($75 \leq t \leq 360$ min). Such a behavior may arise through the effect of randomly distributed defects and impurities which can appear during crystal growth.[41] The presence of defects induc-
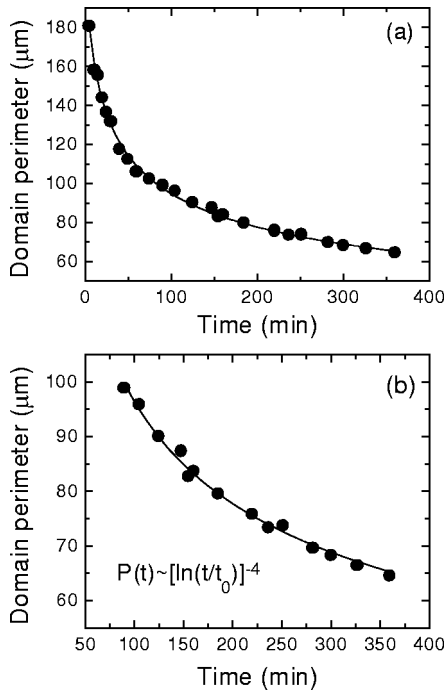
FIG. 6. (a) Time dependence of the total domain perimeter $P(t)$ within a time interval of 360 min. The solid line corresponds to the best fit curve to the power law $P(t) \propto (t-t_0)^\phi$ with $t_0 = -8(1)$ min and $\phi = -0.303(8)$. (b) The fit of $P(t)$, in the late stage of coarsening, to the logarithmic growth law $P(t) \propto [\ln(t/t_0)]^4$.

ing roughening and acting as pinning sites for domain walls may severely slow down the ordering process.[42] In this case, a much slower logarithmic growth law, namely, $L(t) \propto [\ln(t/t_0)]^{1/\psi}$ with $\psi = \chi/(2-\zeta)$, has been predicted, where t_0 corresponds to a microscopic time scale, ζ is the domain wall roughness exponent, and $\chi = 2\zeta + d - 3$ is the exponent for the domain wall pinning energy with d being the spatial dimensionality. For the most plausible case of $d=2$ applying to the present system where domain ordering proceeds mainly through the lateral wall motion, giving rise to two-dimensional nucleation at the phase boundary,[25] the exponent values of $\zeta = 2/3$ and $\chi = 1/3$ have been determined,[42] and hence the growth law becomes $L(t) \propto [\ln(t/t_0)]^4$, a variation which has been experimentally verified for a random exchange ferromagnet[43] and recently a nematic liquid crystal system,[24] as well. In this respect, we have applied the fit of the experimental $L(t)$ data at the late growth stage ($t \geq 75$ min) to the previous logarithmic time dependence. As shown in Fig. 5(b), $L(t)$ can be reasonably well fitted to the latter growth law, implying that pinning forces induced by randomly distributed defects may be responsible for the retardation of the ordering process. It should be noted that the logarithmic time dependence does not produce an equally satisfactory fit of $L(t)$ to the full range of time as the simple power law, thus supporting the differential behavior in the two time regimes.

In order to obtain an independent estimate of the growth law so that the previous behavior can be further substantiated, we have calculated the total domain perimeter $P(t)$ corresponding to the total length of domain walls in the same image sequence. The corresponding temporal variation of $P(t)$ is shown in Fig. 6(a). The total domain perimeter can
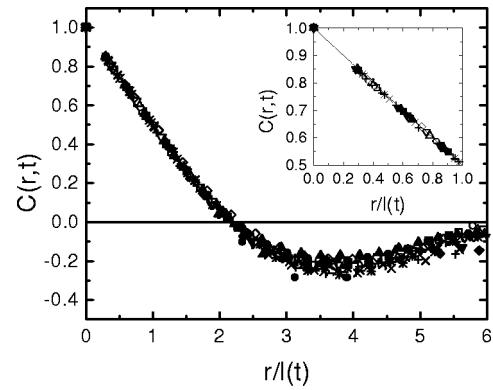

FIG. 7. Scaled correlation functions $C[x \equiv r/L(t)] = f(x)$ of the TGS domain patterns, for all the different times studied. The inset shows the short-distance part of the scaling function $f(x)$ at the same times, following an almost linear behavior of the form $f(x) \approx 1 - 0.5x$ (solid line).

be associated with the correlation length; specifically it is expected to scale as the inverse of the characteristic length $1/L$ which, for the scalar order parameter, is also proportional to the total area of domain walls per unit volume.[23] Fitting of $P(t)$ to the power growth law in the full investigate time range results in the values of $t_0 = -8(1)$ min and $\phi = -0.303(8)$, as shown in Fig. 6(a). Both these values are consistent within error with those derived from the $L(t)$ time dependence, thus verifying the value of $\phi \approx 0.3$ for the growth exponent in the corresponding fit. Accordingly, $P(t)$ exhibits a similar time dependence in the two different time regimes, namely, a faster coarsening rate in the early growth stage and a slower one in the late stage. Fitting of $P(t)$ to the logarithmic time dependence for the late stage may well be obtained, as shown in Fig. 6(b), thus supporting the presence of pinning effects. Based on these results, it appears that domains initially coarsen with a rate close to that predicted for conserved systems and then cross over to a slower logarithmic dependence appropriate for two-dimensional systems with random impurities.

C. Dynamical scaling

Subsequently, we have scaled the distance r by the derived correlation length $L(t)$ in order to examine whether the scaling hypothesis is satisfied in the present system. Figure 7 shows plots of the correlation functions $C(r,t)$ against the scaled distance $r/L(t)$ for all the different times. All plots collapse onto a single curve up to a scaled distance of approximately 2 and then gradually start to disperse, the largest deviation occurring for the latest domain patterns. Such a behavior verifies that the equal-time correlation functions satisfy the dynamical scaling form $C(r,t) = f[x \equiv r/L(t)]$, with x being the scaling variable and $f(x)$ the scaling function which is independent of time and confirms the self-similar morphology for domain growth. Comparison with the scaling functions occasionally reported from simulation of conserved systems[44] or approximate analytical treatments[45] reveals a general agreement of the observed overall $f(x)$ shape, though the calculation of scaling functions for conserved order parameter has been found to impose severe restrictions not fully met with the proposed theories, especially

for scalar fields,[23] as in the present system. The short-distance part of the scaling function $f(x)$ is expected to exhibit a linearly decreasing behavior of the form $f(x) = 1 - \text{const} \times x$, for small scaling variable $(x \ll 1)$.[23] The latter behavior, implying a power-law tail in the structure factor for large wave vector known as Porod's law,[22,23] is a characteristic feature for both conserved and nonconserved scalar fields, reflecting the sharpness of domain walls compared to the average domain size. In order to trace the latter behavior in the TGS system, the short-distance part of the scaled correlation functions $C(r,t)$ is plotted in the inset of Fig. 7. The scaling function indeed decreases in a fairly linear manner, namely, as $f(x) \approx 1 - 0.5x$, indicating that Porod's behavior may apply to the present system.

Explicit calculations have shown that in general the presence of topological defects lead to the singular short-distance behavior of the equal-time correlation function and the power law tail of the structure factor.[46] Exact expressions have been thus derived for the corresponding amplitudes in terms of the defect density, regardless of the nature of the order parameter.[46] In the case of scalar order parameter, the short-distance behavior is predicted to be $C(r,t) = 1 - (2/\pi^{1/2})[\Gamma(d/2)/\Gamma((d+1)/2)]\rho r$, where ρ is the defect density.[23,46] For the case of $d = 2$, the scaling function reduces to the simple form $C(r,t) = 1 - (4/\pi)\rho r$. To obtain a numerical estimate of the linear coefficient of $C(r,t)$ for the present case, the value for the domain wall density ρ, i.e., the domain wall length per unit area, is required. Using the experimental values for $P(t)$ and $L(t)$, the domain wall density is found to scale roughly as $\rho(t) \approx 0.31/L(t)$. Then, within this model, by employing the previous relation for the short-distance part, we find that the scaling function becomes $C(r,t) \approx 1 - 0.4r/L(t)$. On the other hand, the observed linear coefficient appears to be very close to the value of approximately 0.5 predicted for the two-dimensional Ising system,[46] which can be anticipated since the relation for the short-distance singular part of $C(r,t)$ is derived independently of any assumptions for the conservation of the order parameter.[23] It is also worth noting that the effect of random impurities on domain growth does not cause any violation of dynamical scaling, in agreement with predictions following renormalization group arguments[23] suggesting that the scaling functions should be the same as in the pure systems.

D. Charge conservation

To this extent, there is considerable evidence that domain coarsening in TGS proceeds in a self-similar manner with a dominant characteristic length scale consistent with dynamical scaling and a growth law at the early stage of coarsening approaching that for systems with conserved order parameter. Although the order parameter in TGS is the polarization, an earlier NLC study on the submilimeter range[30] has shown that the total surface charge probed by the domain area is conserved within the studied time scale of approximately 90 min. The origin of the latter behavior has been explained considering that when an isolated domain shrinks due to surface tension, the neighboring domains absorb the excess charge and grow, thus maintaining the total surface charge constant. In order to trace the latter behavior we have calculated the area of the two antiparallel domain configura-
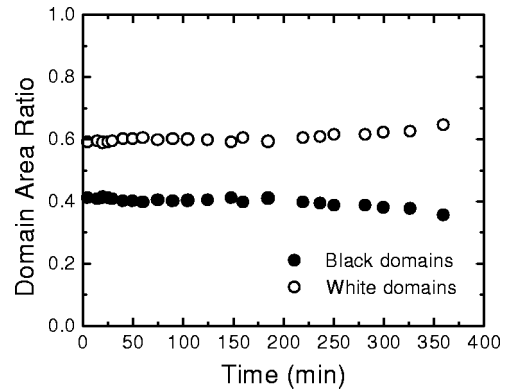

FIG. 8. Time dependence of the domain area ratios normalized to the total pattern area for the two antiparallel domain configurations, here named ''black'' and ''white.''

tions within the same scanning images of 7×7 μm^2, as a function of time. Figure 8 shows the time evolution of the corresponding domain area ratios normalized to the total inspected area. Indeed, the resulting plots confirm that surface charge is conserved on the investigated spatial scale for approximately 360 min. In the present case, where lamellar TGS domain patterns are observed, a similar conservation mechanism, dominated by charge flow in domains of the same polarity after polarization reversal may be claimed. The inequality of the domain area ratios (0.6 to 0.4) reveals a preferential domain orientation which is also maintained in domain images of larger size such as those depicted in Fig. 1, further implying that the total surface charge at the time when nucleation started was not zero. This intriguing asymmetry of the domain distribution might be effectively described by a weak internal bias field that favors one direction of the spontaneous polarization. The origin of such a bias field has been related to anisotropic defect centers introduced in the host lattice of TGS and other ferroelectric materials in the process of crystal growth.[47,48] Moreover, as theoretically argued[23] and experimentally observed,[30] the conservation of the total surface charge and the particular power growth law may hold independently on the volume fraction of the two domain states. On the other hand, the surface charge cannot be conserved forever since the energetically favorable domain configuration for a ferroelectric crystal, when all depolarizing fields are compensated by free or bound charges, is the single domain state. However, the presence of a finite defect concentration may fix the domain structure, stabilize the polarization of the crystal,[41] and thus inhibit domain growth. Therefore, we may conclude that domain ordering dynamics in quenched TGS crystals may exhibit characteristics for systems with conserved order parameter within a certain time period depending on the quality of the crystal and its defect structure. A similar behavior for domain kinetics may be, in principle, anticipated for other ferroelectric materials, as well. However, factors, such as the diversity of the defect structure that depends on the conditions of crystal growth,[41,48] impose the need for further experiments assessing quantitatively domain evolution in both pure and doped ferroelectric materials.

IV. CONCLUSIONS

In conclusion, we have shown that scanning force microscopy employing voltage modulation provides a very effec-

tive method for the real time investigation of domain kinetics in ferroelectric TGS single crystals with high lateral resolution and more specifically of domain growth after a rapid thermal quench from the paraelectric to the ferroelectric phase. The temporal study of the equal-time correlation functions for the TGS domain patterns reveals that the characteristic correlation length increases in the early stage of coarsening according to a power law with growth exponent close to that of conserved systems, $L(t) \propto t^{1/3}$. Further, in the late coarsening stage, the correlation length exhibits a crossover to the logarithmic time dependence $L(t) \approx [\ln(t/t_0)]^4$ predicted for systems with random impurities causing roughening and pinning of domain walls. Domain growth is found to be dominated by a single characteristic length scale consis-

tent with the dynamical scaling hypothesis, while the short-distance behavior of the scaling function complies with Porod's law. Conservation of the total surface charge, probed by the temporal evolution of the domain area, is found to hold within the studied time and spatial scale, indicating that domain dynamics in TGS under favorable conditions may be similar to those of systems with conserved order parameter.

ACKNOWLEDGMENTS

*On sabbatical leave from Dipartimento di Fisica MTFA, Università di Messina, Salita Sperone 31, I-98166 Messina, Italy.

[1] S.L. Swartz and V.E. Wood, Condens. Matter News **1**, 4 (1992); C.H. Ahn, T. Tybell, L. Antognazza, K. Char, R.H. Hammond, M.R. Beasley, Ø Fischer, and J.-M. Triscone, Science **276**, 1100 (1997); D. Damjanovic, Rep. Prog. Phys. **61**, 1267 (1998).

[2] W. Cao and L.E. Cross, Phys. Rev. B **44**, 5 (1991); Y. Ishibashi, Ferroelectrics **98**, 193 (1993).

[3] M.E. Lines and A.M. Glass, *Principles and Applications of Ferroelectrics and Related Materials* (Clarendon, Oxford, 1977).

[4] F. Saurenbach and B.D. Terris, Appl. Phys. Lett. **56**, 1703 (1990).

[5] R. Lüthi, H. Haefke, K.-P. Meyer, E. Meyer, L. Howald, and H.-J. Güntherodt, J. Appl. Phys. **74**, 7461 (1993).

[6] T.J. Yang, V. Gopalan, P.J. Swart, and U. Mohideen, Phys. Rev. Lett. **82**, 4106 (1999).

[7] S. Zhu and W. Cao, Phys. Rev. Lett. **79**, 2558 (1997).

[8] O. Kolosov, A. Gruverman, J. Hatano, K. Takahashi, and H. Tokumoto, Phys. Rev. Lett. **74**, 4309 (1995).

[9] M.-K. Bae, T. Horiuchi, K. Hara, Y. Ishibashi, and K. Matsushige, Jpn. J. Appl. Phys., Part 1 **33**, 1390 (1994).

[10] A. Correia, J. Massanell, N. García, A.P. Levanyuk, A. Zlatkin, and J. Przeslawski, Appl. Phys. Lett. **68**, 2796 (1996).

[11] L.M. Eng, J. Fousek, and P. Günther, Ferroelectrics **191**, 211 (1997).

[12] H. Bluhm, U.D. Schwarz, and R. Wiesendanger, Phys. Rev. B **57**, 161 (1998).

[13] R. Lüthi, H. Haefke, W. Gutmannsbauer, E. Meyer, L. Howald, and H.-J. Güntherodt, J. Vac. Sci. Technol. B **12**, 2451 (1994).

[14] H. Haefke, R. Lüthi, K.-P. Meyer, and H.-J. Güntherodt, Ferroelectrics **151**, 143 (1994).

[15] L.M. Eng, M. Friedrich, J. Fousek, and P. Günther, J. Vac. Sci. Technol. B **14**, 1191 (1996).

[16] H. Bluhm, A. Wadas, R. Wiesendanger, K.-P. Meyer, and L. Szczesniak, Phys. Rev. B **55**, 4 (1997).

[17] J. Ohgami, Y. Sugawara, S. Morita, E. Nakamura, and T. Ozaki, Jpn. J. Appl. Phys., Part 1 **35**, 2734 (1996).

[18] M. Abplanalp, L.M. Eng, and P. Günther, Appl. Phys. A: Mater. Sci. Process. **66**, S231 (1998).

[19] L.M. Eng, M. Abplanalp, and P. Günther, Appl. Phys. A: Mater. Sci. Process. **66**, S679 (1998).

[20] J.W. Hong, K.H. Noh, S.-I. Park, S.I. Kwun, and Z.G. Khim, Phys. Rev. B **58**, 5078 (1998).

[21] J.W. Hong, D.S. Kahng, J.C. Shin, H.J. Kim, and Z.G. Khim, J. Vac. Sci. Technol. B **16**, 2942 (1998).

[22] J.D. Gunton, M. San Miguel, and P.S. Sahni, in *Phase Transitions and Critical Phenomena*, edited by C. Domb and J.L. Lebowitz (Academic, London, 1983), p. 267; H. Furukawa, Adv. Phys. **34**, 703 (1985); K. Binder, Rep. Prog. Phys. **50**, 783 (1987).

[23] A.J. Bray, Adv. Phys. **43**, 357 (1994).

[24] I. Chuang, N. Turok, and B. Yurke, Phys. Rev. Lett. **66**, 2472 (1991); H.M. Shehadeh, and J.P. McClymer, *ibid.* **79**, 4206 (1997); D.K. Shenoy, J.V. Selinger, K.A. Grüneberg, J. Naciri, and R. Shashidhar, *ibid.* **82**, 1716 (1999), and references therein.

[25] V.Ya. Shur and E.L. Rumyantsev, Ferroelectrics **191**, 319 (1997).

[26] F. Suda, J. Hatano, and H. Futama, J. Phys. Soc. Jpn. **44**, 244 (1978).

[27] F. Moravets and V.P. Konstantinova, Kristallografiya **13**, 284 (1968) [Sov. Phys. Crystallogr. **13**, 221 (1968)].

[28] V.P. Konstantinova and I. Stankowska, Kristallografiya **16**, 158 (1971) [Sov. Phys. Crystallogr. **16**, 123 (1971)].

[29] N. Nakatani, Jpn. J. Appl. Phys., Part 2 **24**, L528 (1985); Ferroelectrics **97**, 127 (1989).

[30] N. Tomita, H. Orihara, and Y. Ishibashi, J. Phys. Soc. Jpn. **58**, 1190 (1989).

[31] H. Orihara, N. Tomita, and Y. Ishibashi, Ferroelectrics **95**, 45 (1989).

[32] K. Franke, Ferroelectr. Lett. Sect. **19**, 25 (1995); K. Franke and M. Weihnacht, *ibid.* **19**, 35 (1995).

[33] M. Labardi, V. Likodimos, and M. Allegrini, Phys. Rev. B **61**, 14 390 (2000).

[34] M. Labardi, M. Allegrini, E. Marchetti, and P. Sgarzi, J. Vac. Sci. Technol. B **14**, 1509 (1996).

[35] V. Likodimos, X.K. Orlik, M. Labardi, L. Pardi, and M. Allegrini, J. Appl. Phys. **87**, 443 (2000).

[36] K. Takahashi and M. Takagi, J. Phys. Soc. Jpn. **44**, 1266 (1978).

[37] K. Takata, J. Vac. Sci. Technol. B **14**, 3393 (1996).

[38] N.A. Tikhomirova, A.V. Ginzberg, L.I. Dontsova, S.A. Pikin, and L.A. Shuvalov, Kristallografiya **30**, 330 (1985) [Sov. Phys. Crystallogr. **30**, 191 (1985)]; V.Ya. Shur, A.L. Gruverman, V.P. Kuminov, and N.A. Tonkachyova, Ferroelectrics **111**, 197 (1990).

[39] L.I. Dontsova, E.S. Popov, A.V. Shil'nikov, L.G. Bulatova, N.A. Tikhomirova, and L.A. Shuvalov, Kristallografia **20**, 758 (1981) [Sov. Phys. Crystallogr. **26**, 430 (1981)].

[40] A.J. Bray, Phys. Rev. E **58**, 1508 (1998).

[41] J. Stankowska and A. Czarnecka, Ferroelectrics **98**, 95 (1989).

[42] D.A. Huse and C.L. Henley, Phys. Rev. Lett. **54**, 2708 (1985); D.A. Huse, C.L. Henley, and D.S. Fisher, *ibid.* **55**, 2924 (1985).

[43] A.G. Schins, A.F.M. Arts, and H.W. De Wijn, Phys. Rev. Lett. **70**, 2340 (1993).

[44] A. Shinozaki and Y. Oono, Phys. Rev. E **48**, 2622 (1993); M. Siegert and M. Rao, Phys. Rev. Lett. **70**, 1956 (1993).

[45] A.J. Bray and K. Humanyun, Phys. Rev. Lett. **68**, 1559 (1992); F. Rojas and A.J. Bray, Phys. Rev. E **51**, 188 (1995).

[46] A.J. Bray and K. Humanyun, Phys. Rev. E **47**, R9 (1993).

[47] N. Nakatani and N. Hara, Jpn. J. Appl. Phys., Part 1 **32**, 3204 (1993).

[48] K. Matyjasek and R. Jakubas, Ferroelectrics **190**, 25 (1997).